

Influenza Virus-Membrane Fusion Triggered by Proton Uncaging for Single Particle Studies of Fusion Kinetics

Deirdre A. Costello,[†] Donald W. Lee,[†] Jennifer Drewes,[‡] Kevin A. Vasquez,[†] Cassandra Kisler,[§] Ulrich Wiesner,[‡] Lois Pollack,[§] Gary R. Whittaker,[⊥] and Susan Daniel^{*,†}

[†]School of Chemical and Biomolecular Engineering, Cornell University, Ithaca, New York, United States

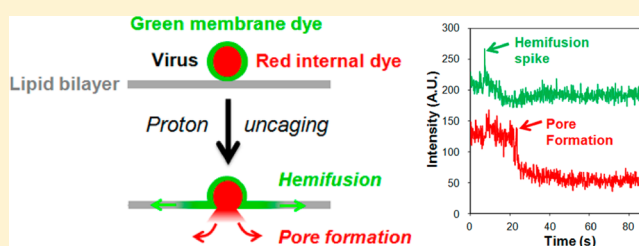
[‡]Department of Materials Science and Engineering, Cornell University, Ithaca, New York, United States

[§]School of Applied and Engineering Physics, Cornell University, Ithaca, New York, United States

[⊥]Department of Microbiology and Immunology, Cornell University, Ithaca, New York, United States

S Supporting Information

ABSTRACT: We report a method for studying membrane fusion, focusing on influenza virus fusion to lipid bilayers, which provides high temporal resolution through the rapid and coordinated initiation of individual virus fusion events. Each fusion event proceeds through a series of steps, much like multistep chemical reaction. Fusion is initiated by a rapid decrease in pH that accompanies the “uncaging” of an effector molecule from *o*-nitrobenzaldehyde, a photoisomerizable compound that releases a proton to the surrounding solution within microseconds of long-wave ultraviolet irradiation. In order to quantify pH values upon UV irradiation and uncaging, we introduce a simple silica nanoparticle pH sensor, useful for reporting the pH in homogeneous nanoliter volumes under conditions where traditional organic dye-type pH probes fail. Subsequent single-virion fusion events are monitored using total internal reflection fluorescence microscopy. Statistical analysis of these stochastic events uncovers kinetic information about the fusion reaction. This approach reveals that the kinetic parameters obtained from the data are sensitive to the rate at which protons are delivered to the bound viruses. Higher resolution measurements can enhance fundamental fusion studies and aid antiviral antifusogenic drug development.



Fusion of cell membranes is a ubiquitous biological process involved in vesicle fusion to membrane synapses, fertilization between sperm and egg cells, the merging of intracellular lysosomes, and membrane-enveloped virus fusion to endosomes.¹ The fusion step is critical to the delivery of material across membranes. For example, in virus infection, membrane-enveloped viruses, such as influenza, infect cells via the endocytotic pathway, which necessitates the merging of the viral membrane with the endosomal membrane to pass viral genetic material into the cytosol. For many enveloped viruses, a drop in endosomal pH triggers conformational changes in the viral coat proteins required to initiate fusion between the viral and endosomal membranes.² Characterization of virus fusion kinetics is important for a number of reasons beyond understanding fundamental fusion processes, such as classification of viral strain virulence and in the development of antifusogenic drugs.³ Yet, directly studying fusion *in vivo* is difficult because it occurs inside intracellular compartments that are cumbersome to control and assay. Therefore, much of what is known about virus fusion has been determined using bulk or ensemble *in vitro* fusion assays that report on the collective fusion behavior of many viruses to model membranes.^{4–14}

In bulk fusion assays, virus fusion is typically reported by a collective change in intensity resulting from fluorescence

dequenching upon fusion of an ensemble of fluorescently labeled viruses to model membranes.^{4–14} Fusion is initiated by acidification of the bulk solution. From the resulting temporal change in the fluorescence signal, some information about the kinetics of virus fusion can be obtained. Many studies of virus fusion to date have been conducted using this type of assay,^{4–14} but there are significant limitations with this approach. First, because individual events cannot be observed in this assay, viral binding and fusion cannot be distinguished from each other; this constraint impedes the separation of transport limitations from the fusion kinetics. Second, as the output signal is an aggregate of fluorescence changes resulting from many stochastic fusion events, only averaged information can be obtained from these assays; this drawback can obscure processes that occur at shorter time scales. Third, temporal limitations in uniformly acidifying the solution can spread initiation times of individual events, impacting signal response and its analysis. This limitation can reduce the temporal resolution of the measurements and obscure the sensitivity of initiating pH on kinetics.¹⁵

Received: March 5, 2012

Accepted: September 14, 2012

Published: September 14, 2012

Direct observation of individual virus fusion events circumvents many of the drawbacks of ensemble methods. Single particle virus fusion methods were first developed around the early 1990s^{16–18} and have improved significantly since then with modern electronics and optics capable of single molecule fluorescence detection, microfluidic approaches for fluid handling, and new strategies for creating robust membranes. More recent work has provided information on the kinetics of intermediate steps of the fusion mechanism by employing total internal reflection fluorescence microscopy (TIRF)¹⁹ to detect individual virus fusion events to solid-supported lipid bilayers (SLBs) adsorbed to the walls of microfluidic devices.^{20,21} Although today's single particle virus fusion studies are easier to implement and can provide more insight into virus fusion than previously possible, two significant limitations of this approach remain: the rate at which acidification can be achieved in the confined space of the microfluidic device via acidic buffer exchange and the subsequent shearing that is imposed in the channel due to the flow.

Here, we describe a method to achieve rapid acidification under quiescent conditions by integrating a photoisomerizable compound, *o*-nitrobenzaldehyde (*o*-NBA), into our single particle fusion assay. *o*-NBA donates a proton to the surrounding solution when illuminated with a 355 nm long-wave ultraviolet laser²² with release times on the order of microseconds.²³ This acidification method will hereafter be referred to as "proton uncaging". The photolysis of *o*-NBA to create a pH jump has been used in the investigation of the mechanisms of biological systems because it offers very high time resolution for kinetic measurements. In a review by McCray et al.,²² applications for uncaging are highlighted that include the study of active transport of proteins in muscle fibers, mechanistic studies of ion channels, and time-resolved responses of bacterial flagella motors to rapid changes in extracellular pH. Abbruzzetti et al.²⁴ used it to examine the dissociation kinetics of histidines in Gu HCl-unfolded Fe(III) cytochrome C to increase the temporal resolution of data acquisition and allow for investigation over a wider temperature range. Saxena et al.²⁵ studied the kinetics of proton transfer in green fluorescent protein (GFP) using *o*-NBA, as a model system for characterizing the correlation between dynamics and function of proteins in general. Each of these examples illustrates the advantages of using a rapid pH jump to study pH-dependent kinetic processes. To the best of our knowledge, however, uncaging has not yet been employed for the study of pH-dependent fusion kinetics of enveloped viruses to host membranes.

There are several advantages of an uncaging strategy that are particularly beneficial for kinetic studies of viral fusion. First, the rate of release of the effector molecule (a proton) is much faster than rapid exchange of solution. Second, the effector molecule can be released close to the target, i.e., the fusion protein. Increasing the certainty of when the acidification occurs and ensuring the coordinated initiation of fusion events improves the resolution of fusion kinetics. Uncaging times are much faster than the protein conformational change for influenza hemagglutinin (HA) X:31 at the optimum triggering pH of ~ 5.0 .²⁶ A third advantage is that the environment in which the dynamics are studied is unperturbed by external forces resulting from hydrodynamic flow. The quiescent surroundings more closely mimic the endosomal environment and eliminate the possibility of hydrodynamic deformation of protein structures, which could (slightly) change the conformation of the protein—

receptor complex and impact fusion kinetics. Fourth, the absence of flow makes it possible to follow multiple processes (e.g., binding, hemifusion, pore formation) within an individual virion without it leaving the field of view.

By adjusting the concentration of *o*-NBA, the triggering pH immediately following uncaging can be tuned to achieve pH values within the range of physiological fusion pH for influenza. The characterization of the pH change in nanoliter volumes is a challenge, however, as the UV irradiation triggering proton uncaging also typically bleaches pH sensing reporter dyes. In order to be able to quantify pH, a more UV resistant sensor probe thus had to be developed.

■ MATERIALS AND METHODS

The sources of all materials and detailed methods, image processing, and data analysis are described in the Supporting Information. Described here are the major features of the assay and its execution.

Supported Lipid Bilayers. The following lipids were used in these experiments: 1,2-dioleoyl-*sn*-glycero-3-phosphocholine (DOPC), 1-palmitoyl-2-oleoyl-*sn*-glycero-3-phosphocholine (POPC), cholesterol, and total ganglioside extract (bovine, brain). Lipid vesicles were prepared using a molar ratio of 4:4:2:0.5 of DOPC, POPC, cholesterol, and total ganglioside extract. For acidic flow experiments, 0.01 mol % Oregon green DHPE lipid was added to the bilayer formulation to signal the pH drop. A detailed procedure for making liposomes used to form the supported bilayers and characterization can be found in the Supporting Information.

Virus Labeling. Influenza X:31 (H3N2) with a hemagglutinin (HA) concentration of 2 mg/mL (as determined by Charles River Laboratories) was used in all experiments. Virus membranes were labeled with lipophilic fluorophores, octadecylrhodamine B chloride (R18), a red-emitting fluorophore, or Rhodamine 110 octadecyl ester (R110C18), a green-emitting fluorophore, at sufficient concentrations to (semi-) quench fluorescence, following slight modifications to standard procedures^{4,27} as described in the Supporting Information. Virus internal contents were labeled with Sulforhodamine B (SRB), a red-emitting fluorophore, as described in the Supporting Information.

C Dot pH Sensor Synthesis and Characterization. Fluorescent core-shell silica nanoparticle (Cornell or C dots) sensors were synthesized via a modified Stöber synthesis.^{28,29} In contrast to earlier ratiometric two-color sensor particles,^{30,31} here, only single-color C dot sensors were required as pH sensing was performed in environments homogeneous on the length scale of the optical microscope resolution. To that end, first, Oregon green maleimide was conjugated with MPTMS at a molar ratio of 1:50 (dye/MPTMS) in dimethyl sulfoxide under nitrogen for 12 h. The dye conjugate solution was then added to an ethanolic solution of 0.02 M ammonia and 4.275 M deionized water at a final concentration of 1.7×10^{-5} M dye conjugate. To this, a pure silica precursor, tetraethylorthosilicate, TEOS, was added at a concentration of 0.05 M. After reacting for 12 h, the cores were coated with a shell of additional TEOS (0.140 M) added in 31 equal aliquots at 10 min intervals. The C dots were allowed to react for 12 h after the shell addition and were then dialyzed to deionized water. The particles in water were then densified by heating at 120 °C in a tightly sealed reaction vial for 48 h. This postsynthesis densification step provided improved UV stability of the encapsulated dye (data not shown). The final size of the single-

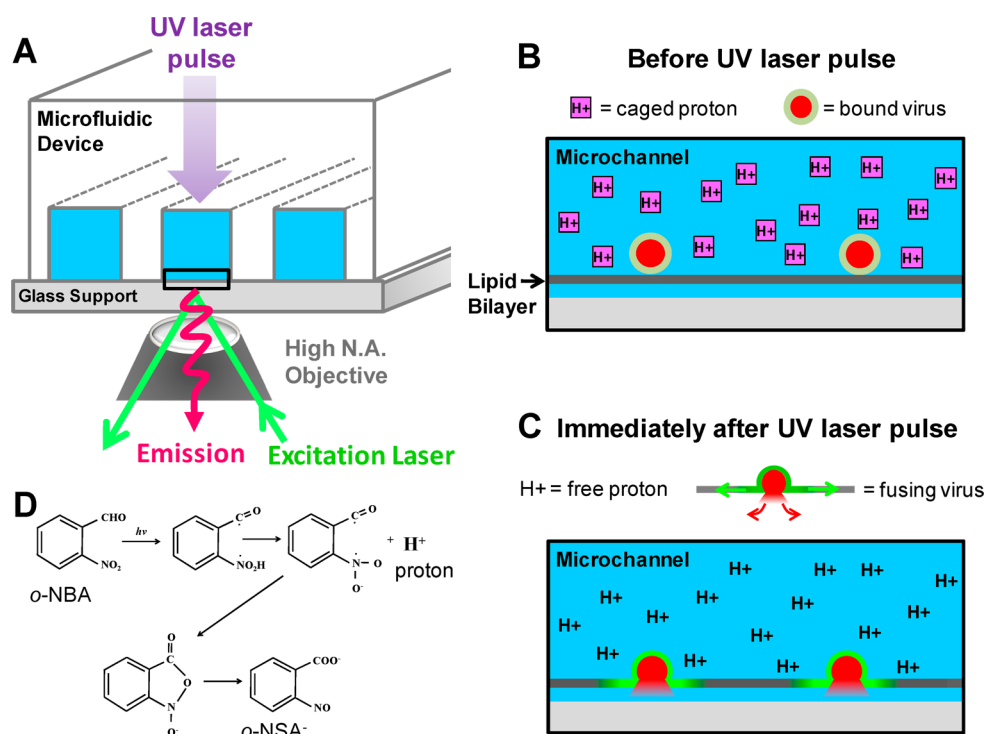


Figure 1. (A) An illustration of the microfluidic device coupled to a TIRF microscope for imaging individual virion fusion events. The purple arrow entering the top of the device represents a UV laser that is aligned directly with the microscope objective beneath the device. Note that the dimensions of this drawing are not to scale. The actual channel is about $130\ \mu\text{m}$ wide by $70\ \mu\text{m}$ high, and the diameter of the UV laser beam is about $100\ \mu\text{m}$. (B) An inset of the region within the field of view of the camera, drawn as the black rectangle in (A), prior to UV irradiation at a neutral pH. This illustration shows that the glass surface comprising the fourth wall of the microchannel is coated with a solid supported lipid bilayer (gray). Virus labeled with a quenching concentration of fluorophore is colored light green with a red interior. The dark pink boxes represent proton cages (*o*-NBA) that release protons when illuminated with 355 nm light. Note that this drawing is also not to scale; influenza virus is typically $100\ \text{nm}$ in diameter, and the bilayer is $\sim 4\ \text{nm}$ thick. (C) Immediately following UV irradiation, the caged protons are released (denoted as free H^+ in the diagram), acidifying the surrounding solution. Fusing viruses are now colored bright green to denote the dequenching of green fluorophores and the escape of the internal red dye upon pore formation. (D) The photochemistry of uncaging: the conversion of *o*-nitrobenzaldehyde to *o*-nitrosobenzoic acid and a proton upon irradiation with UV light. Adapted from ref 35. Copyright 1980 American Chemical Society.

color C dots sensor was determined by dynamic light scattering using a Malvern Zetasizer Nano, indicating an average diameter of $28\ \text{nm}$.

TIRF Microscope Configuration. Fusion assays were carried out using total internal reflection fluorescence microscopy using an inverted Zeiss Axio Observer.Z1 with a α Plan-Apochromat $100\times$ oil objective with a numerical aperture (NA) of 1.46. Index-matching liquid (Carl Zeiss, Inc.) was used to couple the glass coverslip of the flow cell device to the objective. In this setup, two lasers can be used simultaneously to excite different color fluorophores; we used 561 and 488 nm excitation wavelengths from solid-state lasers. These were coupled into the optical pathway of the microscope using a Laser TIRF 3 slider (Carl Zeiss, Inc.), which controlled the angles of incidence. Exceeding the critical angle ($\sim 62^\circ$) ensured total internal reflection of the lasers and created evanescent waves about $100\ \text{nm}$ thick. The evanescent waves excited fluorescently labeled virus bound to sialic acid groups of the ganglioside lipids comprising the lipid bilayers, which was positioned within several nanometers of the glass–water interface. The excitation laser light was band-pass filtered through a Semrock 74 HE GFP/mRFP filter cube and then combined with a dichroic mirror before being focused on the outer edge of the back aperture of the objective. The fluorescence emission signal was filtered through a 525/31 and 616/57 nm dual band-pass emission filter and then sent to

an electron multiplying CCD camera (Hamamatsu ImageEM C9100-13, Bridgewater, NJ). For acid flow and dual labeling experiments, the emission was passed through a splitter (Photometrics DV2) to divide and focus green and red channels onto separate regions of the EMCCD camera.

Execution of the *o*-Nitrobenzaldehyde Proton Uncaging Assay. Supported lipid bilayers were formed in the flow cell via vesicle fusion^{32–34} by drawing a 10% dilution of liposomes into each channel at a flow rate of $100\ \mu\text{L}/\text{min}$ for 1 min using a syringe pump (PHD 2000 Infuse/Withdraw, Harvard apparatus, Holliston, MA). After 1 min, the flow rate was reduced to $10\ \mu\text{L}/\text{min}$ for 10 more minutes and then stopped to allow the channel to incubate for an additional 10 min. After this incubation, a fresh solution of liposomes was drawn into the channels and incubated for an additional 5 min to ensure a defect-free bilayer and complete coverage of the channel walls. The channels were then rinsed with buffer A (150 mM NaCl, 1.5 mM MES, 5 mM citric acid) for 2 min at $100\ \mu\text{L}/\text{min}$ to remove unfused liposomes. Labeled virus was then pumped into the channels at $30\ \mu\text{L}/\text{min}$ and allowed to incubate for 20 min. After the first incubation, additional virus was pumped into the channels, incubated for 10 min, and repeated until the desired surface density was reached. After the final incubation, *o*-NBA solution (for buffer B, see Supporting Information for preparation) was drawn into the channels at $100\ \mu\text{L}/\text{min}$ for 3 min. We note that no fusion was observed

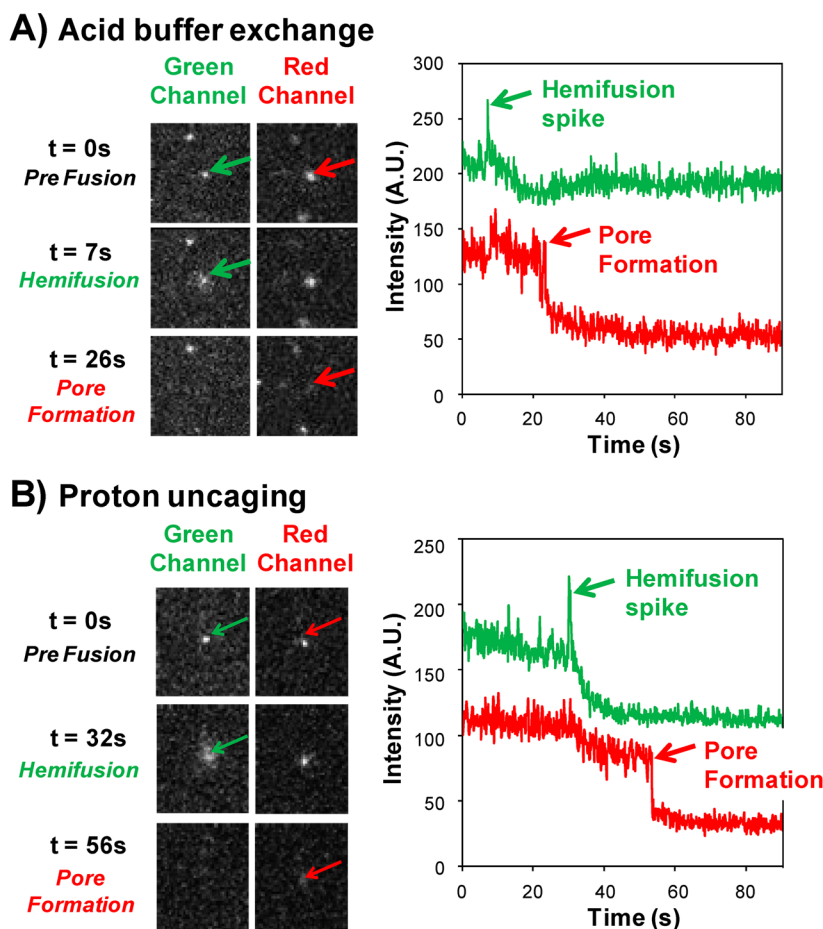


Figure 2. (A) Virus fusion initiated by acidic buffer flow exchange. Green and red fluorescence images of a single fusing virus, marked by the arrows. After acidification, the green channel shows the hemifusion of the membranes; the spike in fluorescence is observed in the plot to the right. The red channel shows the radial diffusion of the internal red fluorophore after pore formation. The drop in red signal can be observed in the plot to the right; here, it takes ~ 20 s between hemifusion and pore formation. (B) Virus fusion initiated by proton uncaging. Here, it takes ~ 15 s between hemifusion and pore formation.

during the flow steps in any assay at any condition we used. The *o*-NBA solution was then incubated in the channel for 20 min to reduce any residual convection in the channel after pumping ceased.

The pH drop was initiated by irradiating a $100\ \mu\text{m}$ diameter section of the channel with a 4 mW UV laser for 200 ms. The beam diameter was measured to be approximately $100\ \mu\text{m}$; thus, when the beam was centered in the field of view of the microscope, it actually covered an area greater than the field of view. We ensured that the uncaging was uniform by mapping out the fusion events across the field of view in time, as shown in Figure S1 in Supporting Information. The alignment of the laser is critical to ensuring that the uncaging is not biased; this can be achieved using a fluorescently labeled bilayer in an extra channel to map out the precise alignment prior to uncaging in virus-filled channels. Using this method, the time of the pH drop is known precisely, as the cleavage of protons from the *o*-NBA molecules occurs on the order of microseconds.²³ The lag between the closing of the UV shutter and the opening of the camera shutter was 200 ms. The UV flash time was 200 ms. Because of the accurate time control of this technique, it removed the requirement for a pH sensitive fluorescent probe to be present in the lipid bilayers to mark when the change in pH occurred. These probes can potentially interfere with the fusion and increase background noise in the images. Hemi-

fusion lag times are defined as the time elapsed between acidification of the field-of-view and fluorescence dequenching for individual virus particles. Pore formation lag times are defined as the time between the start of the hemifusion step and the start of the release of the internal viral fluorophore.

The deprotonation of *o*-NBA resulted in a pH decrease from 7.0 to 5.4, 4.9, or 4.6, depending on the amount of *o*-NBA added to the buffer (see Supporting Information for exact formulations of the buffers). Fluorescence images of the viral fusion events were collected at 50 ms intervals for 2 min. In a few cases, images were taken for longer times to ensure all fusion events were captured within the typical 2 min acquisition time.

Execution of the Acidic Buffer Flow Exchange Assay.

In this experiment, the formation of bilayers, virus binding, and rinsing steps were conducted as described above. Here, instead of initiating hemifusion using the proton uncaging method, hemifusion was initiated by flowing buffer A (150 mM NaCl, 1.5 mM MES, 5 mM citric acid) precalibrated over a range of low pH values into the flow-cell at a flow rate of $100\ \mu\text{L}/\text{min}$ for 2 min. The time at which acidification of the flow cell occurred was marked by a decrease in fluorescence of Oregon green DHPE present in the supported bilayer for this purpose. Images were collected at an interval of 100 ms for 3 or 4 min.

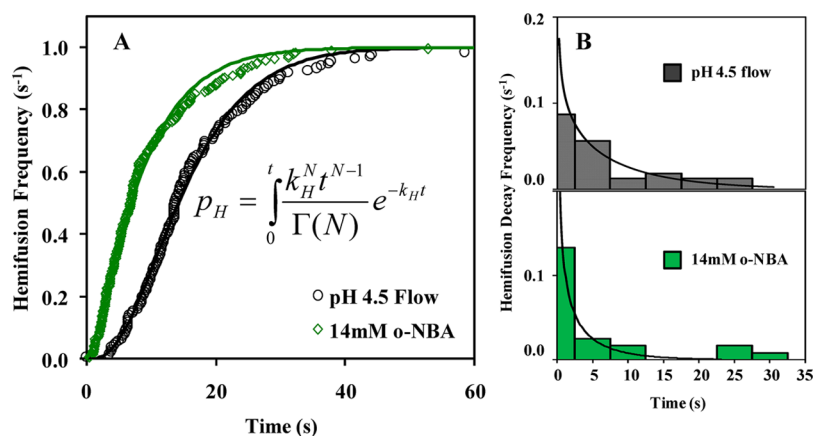


Figure 3. (A) Frequency of hemifusion events plotted as a function of time for initiation pH 4.5 obtained either by acidic buffer exchange (open black circles) or by proton uncaging using 14 mM *o*-NBA (open green diamonds). The lines are the best fits to gamma function equation shown in the inset and are described in detail in the Supporting Information. The rate of hemifusion, k_H , was $0.20 \pm 0.01 \text{ s}^{-1}$ and $0.17 \pm 0.01 \text{ s}^{-1}$ for acidic buffer exchange and proton uncaging, respectively. N values for acid exchange and uncaging are $3.2 \pm 0.1 \text{ s}^{-1}$ and $1.51 \pm 0.05 \text{ s}^{-1}$, respectively. (B) Histograms of lag times between the onset of hemifusion and the onset of pore formation. (Top) Acidic buffer exchange; (Bottom) proton uncaging. The rate of transition from hemifusion to pore formation ($k_{H \rightarrow P}$) using the acid flow and uncaging methods was found to be $0.08 \pm 0.02 \text{ s}^{-1}$ and $0.09 \pm 0.05 \text{ s}^{-1}$, respectively. N was less than 1 in both cases (0.7 ± 0.1 for acid flow and 0.5 ± 0.1 for uncaging), which agrees with previous findings that there is a single step transition between hemifusion and pore formation.

RESULTS AND DISCUSSION

Individual Virion Fusion Assay. We monitored individual influenza X:31 (H3N2) virus fusion events occurring inside a microfluidic device that had its walls coated with supported lipid bilayers to mimic the endosomal membrane. Supported lipid bilayers have served as excellent cell membrane mimics in numerous applications since their introduction in the 1980s³² because they are chemically tunable and preserve the two-dimensional fluidity of constituents. This fluidity is key, as influenza is capable of multivalent binding to sialic acid receptors present in the bilayer. In this application, we employed a bilayer containing a mix of sialic receptors for virus binding. Once the bilayer formed in the device, fluorescently labeled virus was introduced into the channel and bound to the supported bilayer as described in Materials and Methods.

The microfluidic device was coupled to a total internal reflection fluorescence microscope, as illustrated in Figure 1A, and used to image the individual virus fusion events. After fusion initiation by acidification, fluorescence dequenching of a green fluorophore in the viral membrane signals the onset of the merging of the opposing leaflets of the virus and the supported bilayer, called “hemifusion.” The fluorescent “spike” and “cloud” features are easily monitored with TIRF^{20,21} because TIRF is a surface-specific technique that effectively eliminates any fluorescent signal from the bulk that might obscure single fusion events. Pore formation is marked by radial diffusion of a red fluorophore originating from inside the virus, colocalized with the green fluorophore. A sequence of images showing these features is given in Figure 2A and is described in more detail in the Supporting Information. A movie of virus fusion is also provided in the Supporting Information.

The fusion process is hypothesized to occur in several steps.^{12–14,36,37} First, the viral fusion protein, HA, undergoes a conformational change from a prefusion folded state to an extended state, exposing hydrophobic fusion peptides which insert into the host membrane. This intermediate undergoes an additional conformational change which brings the two distal leaflets of each membrane close to each other, causing them to

merge. Merging of the outer leaflets results in the creation of a hemifusion stalk, aided by the concerted action of several HA trimer units. We will hereafter refer to this coordinated unit as a “fusogenic complex.” Eventually, this structure transforms into a fusion pore through which the viral RNA escapes the endosome and enters the cytosol of the cell. Each step and conformational intermediate has a characteristic lifetime; here, we focus on measuring the kinetic rate constant leading up to the hemifusion step and the lag time for pore formation following hemifusion. In this work, we compare the fusion of fluorescently labeled influenza virus to solid-supported lipid bilayers inside microfluidic channels initiated by the traditional acidification method (acidic buffer exchange by flow) and the proton uncaging method (Figure 1).

Single Particle Fusion Assay Using Acidic Buffer Flow Exchange to Initiate Virus Fusion. As both a validation of our assay setup and a control case, we initiated virus fusion by acidic buffer exchange, i.e., by flowing an acidic buffer through the microfluidic channel, not by uncaging. Initially, virus was introduced into the microfluidic device at pH 7.0 and allowed to bind. Unbound virus was gently rinsed from the channel with buffer at pH 7.0. Subsequently, citric acid buffer at various pHs was sent through the channels at a rate of $100 \mu\text{L}/\text{min}$. We chose this specific flow rate for several reasons. First, we wanted to match conditions as closely as possible with previously published reports.²⁰ Second, we selected this moderate flow rate as a compromise between fast flow (for rapid delivery of protons) and slow flow (to minimize shear rates). The rate of buffer exchange must be low enough to minimize tearing viruses off the receptors and/or stretching of the protein conformations which could cause non-native fusion protein–proton interactions and impact kinetics. Balancing these constraints, the $100 \mu\text{L}/\text{min}$ flow rate leads to acidification times for the field of view at 100 \times magnification of several seconds, as measured by the drop in fluorescence of a pH-sensitive fluorophore (Oregon green DHPE) doped into the supported bilayer. Images of the field of view were acquired just before and during acidification at 100 ms intervals. All fusion events within the field of view were recorded and cataloged by

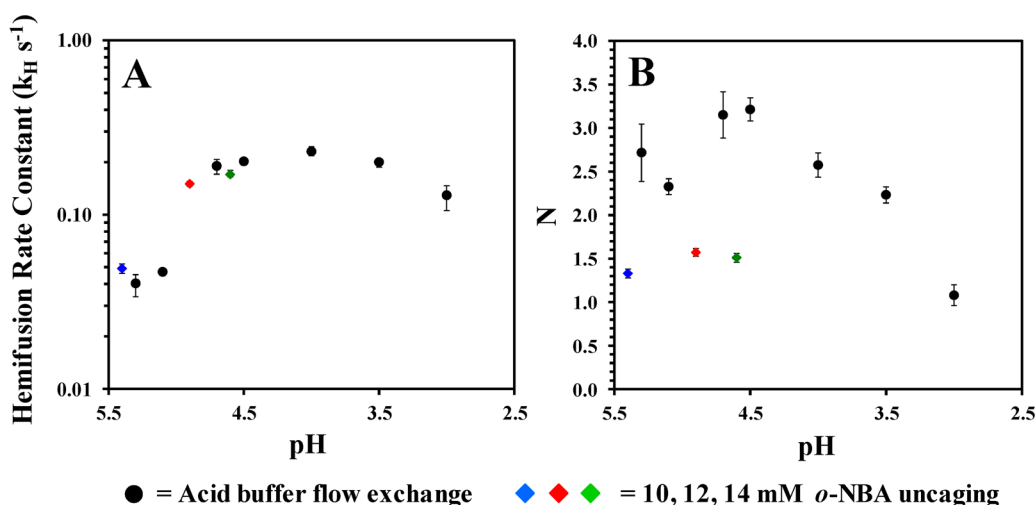


Figure 4. (A) Hemifusion rate constants, k_H , and (B) N parameters for a range of fusion initiation pH values.

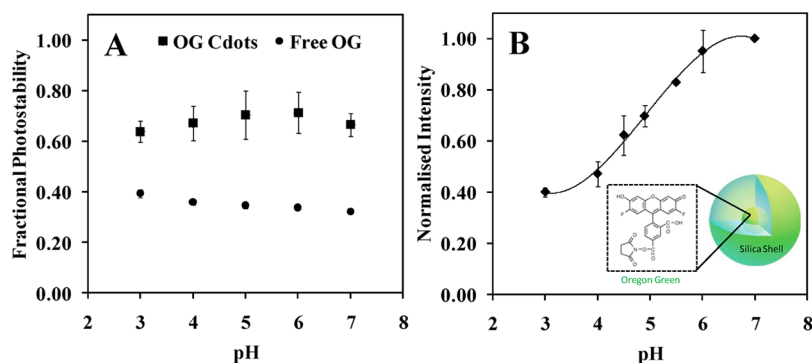


Figure 5. (A) Comparison of photobleaching between Oregon green C dots sensor and free Oregon green after exposure to UV light for 200 ms. Note that the error bars in the free OG case are within the data point. All values are normalized to the intensity value before the 200 ms UV bleach to obtain a fractional photostability at each pH. (B) Calibration curve for Oregon green C dot sensor fluorescence intensity at various pH values. All data were normalized to the pH 7.0 value so that intensities post-UV irradiation could be compared directly. Note that these data were taken after irradiating the samples with UV light to account for photobleaching in the uncaging runs. (Inset) Structure of the Oregon green C dot.

the time point at which the dequenching spike occurred immediately following acidification. A representative set of data for the frequency of events as a function of time after acidification using acid buffer exchange is shown in Figure 3A (open black circles). These data were fit with a cumulative gamma distribution as described in the Supporting Information. Hemifusion kinetic parameters were determined from the best fits of the data for various initiating pHs, as shown in Figure 4 (black circles). The good agreement with previously reported values,²⁰ using the same experimental conditions, validates our assay and provides a point of comparison for the uncaging acidification strategy examined later.

The lag time between the hemifusion step and pore formation was also monitored. Previous work under similar experimental conditions has shown that pore formation lags hemifusion on the order of tens of seconds²⁰ and that this step is independent of pH.^{13,20} A histogram for the pore formation lag time for one set of data taken at pH 4.5 is shown in Figure 4B (top) and agrees with previous work. We note that, in our case, however, a polymer cushion was not used to support the bilayer as employed in previous work.²⁰ Despite this, our results are quite similar indicating that the polymer cushion may not be necessary for this assay. Eliminating this cushion preparation step can reduce the assay preparation time greatly.

To compare these results to the proton uncaging acidification strategy, it is imperative to know the pH following the uncaging event, but to our knowledge, there is no published characterization of the postirradiated pH following uncaging, most likely because no reporter probe existed that could withstand the high energy irradiation of UV without significant photobleaching. Therefore, we first report results obtained from a simple pH-sensing probe we developed to calibrate the pH in nanoliter volumes that can withstand the UV irradiation conditions in our experiment. pH-sensing single-color C dots are composed of Oregon green fluorophore encapsulated in a silica core and surrounded by a pure silica shell. As described in the Materials and Methods section, these C dots sensors were densified in a postsynthesis heating step. Our rationale for this dye-encapsulation approach was based on the fact that (i) silica is known to absorb (and therefore shield from) UV radiation and (ii) the C dot architecture is known to improve photobleaching behavior of organic chromophores through its rigid silica matrix.³⁸ Such particles may also find uses as pH sensors in small volumes in other microfluidic or in vivo applications (e.g., endosomal pH monitoring) or as novel UV sensors beyond the application presented in this work.

Comparison of pH-Sensing Sensitivity between Free Oregon Green and Silica-Encapsulated Oregon Green after UV irradiation. Release of protons from o -NBA occurs

within microseconds²³ when illuminated with 355 nm wavelength light. A pulsed diode pumped solid state laser by Teem Photonics (Model # SNV-04P-000, Lafayette, CO) was used to initiate proton uncaging in the microfluidic device. Uniformity of laser illumination was confirmed by mapping the virus fusion event location in the field of view and noting that the events were random (Supporting Information). The pH in the microfluidic channel after the 200 ms UV pulse was measured using the pH sensitive C dot sensors encapsulating Oregon green. We note here that free Oregon green (devoid of a silica shell) suffered significant photobleaching from the UV pulse and thus could not be used as a pH sensor in this application. Other pH-sensitive fluorophores we tried also failed due to significant photobleaching. Figure 5A compares the level of photobleaching of free Oregon green and the silica-encapsulated Oregon green. This figure clearly shows that the silica capsule protects the Oregon green from photobleaching and that the level of photobleaching is not dependent on the pH of the solution.

Calibration of the Final pH after Irradiation of *o*-Nitrobenzaldehyde Buffer with UV Light Using C Dots.

Solutions of single-color C-dot sensors were prepared in buffer C (1.25 mM MES, ranging from pH 3 to 7). These solutions were loaded into microfluidic channels and imaged under quiescent conditions. Each channel containing a different pH solution was exposed to a 200 ms UV pulse, and images were acquired at an exposure time of 100 ms for 1 min. A calibration curve matching fluorescence intensity to pH (Figure 5B) was generated by normalizing the post-UV bleach intensity value of each solution to the post-UV bleach intensity at pH 7 according to the following equation:

$$I_{\text{calibration}} = \frac{I_{\text{bleach}}^{\text{pHX}} - I_{\text{background}}}{I_{\text{bleach}}^{\text{pH7}} - I_{\text{background}}} \quad (1)$$

where pHX is the pH of the calibration solution or the 10, 12, or 14 mM solution of *o*-NBA in buffer C. The pH post-UV pulse was then determined by matching the normalized intensity for each *o*-NBA concentration to the corresponding pH on the calibration curve. Note that this calibration curve matches well to the published Oregon green pH response curve³⁹ and indicates that as expected the presence of the silica shell does not impede the pH sensing ability of the Oregon green molecule.

It should be noted that the pH reported in Table 1 is the pH approximately 200–300 ms after the UV pulse, as there is a lag

Table 1. Post-UV pH Calibration Table for Various Cage Solutions

concentration of <i>o</i> -NBA in buffer	10 mM	12 mM	14 mM
intensity value	0.83 ± 0.12	0.69 ± 0.06	0.63 ± 0.01
pH from calibration curve	5.4 ± 0.5	4.9 ± 0.2	4.6 ± 0.1

time between the laser shutter closing and the detector turning on. This delay may contribute to the variation in the measurements, as it is possible that the exact pH in the irradiated zone just after the laser hits is slightly lower than what we report here due to the diffusion of any unbound protons along the length of the channel. Because the entire channel is not irradiated with the UV light, the pH in the irradiated zone will recover (see Supporting Information for

details on recovery characteristics in this device). Previous work has shown, however, that the steps following the initial conformational change of the protein induced by low pH do not require a low pH environment themselves;^{13,14} therefore, recovery postfusion initiation should not impact the kinetics obtained. Our work corroborates this previous work, as will be discussed later. All experiments were conducted at ambient temperature (~23 °C).

Single Particle Fusion Assay Using Proton Uncaging to Initiate Virus Fusion. In this set of experiments, acidification was achieved by proton uncaging. The chemical reaction upon UV excitation of *o*-NBA is shown in Figure 1D: *o*-NBA undergoes an intramolecular proton transfer reaction and is converted to a nitronate ion and a proton. The nitronate ion is then converted to an *o*-nitrosobenzoic anion.⁴⁰

In these experiments, virus was introduced into the microfluidic device at pH 7.0 and allowed to bind, as previously described. Buffer at pH 7.0 containing a precalibrated amount of *o*-NBA was used to rinse out the unbound virus. Next, a small region of the channel, prealigned with and encompassing the field of view of the microscope objective, was irradiated for 200 ms with 355 nm light from a solid state UV laser to “uncage” the proton of the *o*-NBA, as shown in Figure 1A,B. Immediately preceding and following irradiation, images were recorded at 50 ms intervals. Fusion events were detected and cataloged using the same procedure described previously for the acidic buffer exchange. A typical set of images of virus fusion initiated by proton uncaging acidification is shown in Figure 2B. Values for k_{H} and N obtained from best fits of the data at various initiating pHs for buffer exchange (flow) acidification and uncaging are reported in Figure 4.

Comparing the results from the two experiments, there are important similarities and differences depending on the acidification method used (Figure 4). Interestingly, k_{H} stays about the same, regardless of the acidification method; however, N is reduced. N is often interpreted to be the number of protein trimers that must act concertedly to initiate fusion.^{20,41} Several previous studies report a value of around three for hemifusion to occur,^{20,42,43} although prior literature includes the possibility that it could be as low as one⁴⁴ or as high as six.^{45,46}

There are several possibilities that could impact fusion kinetics and explain the lowering of N in the uncaging experiment relative to the acidic buffer exchange method. These include: (1) changes in the virus fusion machinery caused by UV irradiation, (2) interactions of the *o*-NBA or the reaction product, *o*-NSA⁻, with the fusion protein, (3) a significant change (drop) in the overall number of particles fusing per experiment (extent of fusion) that affects kinetic analysis, and (4) changes in the delivery rate of protons to the fusion proteins (leading to better coordination of initiation of events, more certainty of when the pH dropped, and elimination of shear effects). To identify the cause of the change, we ran a series of control experiments. A brief summary of the results is presented here only; the details and results of these control experiments are provided in the Supporting Information.

Impact of UV Irradiation on Kinetics. To ensure that UV irradiation itself does not trigger hemifusion or enhance fusion kinetics, a flow cell was prepared under the same experimental conditions as described previously for the proton uncaging experiment, except that it did not contain *o*-NBA. The flow cell was irradiated with the UV laser for 200 ms, and then, images

were acquired at a rate of 200 ms post-UV irradiation. No fusion events were detected. Following this data acquisition, fusion was induced by flowing acidic buffer at pH 5.1 into the channel. In this part of the experiment, hemifusion occurred as previously reported in the acidic buffer exchange experiments, indicating that prior exposure to long wave UV radiation did not affect the ability of the prebound viruses to fuse, in accordance with prior literature.⁴⁷ k_H obtained for these conditions was $0.07 \pm 0.003 \text{ s}^{-1}$ with N value of 2.2 ± 0.10 .

Impact of *o*-NBA or *o*-NSA⁻ on Fusion Kinetics. To ensure that the presence of *o*-NBA or *o*-NSA⁻ did not alter the fusion kinetics, we conducted fusion experiments in exactly the same way as described previously for acidic flow experiments, except the virus was incubated with either *o*-NBA or *o*-NSA⁻ (both at pH 7.0) for 30 min prior to acidic buffer flow exchange. Upon acidification by acidic buffer exchange, the kinetic parameters obtained were nearly the same as in the absence of these compounds. The respective values of k_H and N obtained for each case were 0.17 ± 0.006 and 2.1 ± 0.07 and 0.21 ± 0.01 and 2.9 ± 0.14 . Thus, we confirmed that the presence of *o*-NBA or *o*-NSA⁻ did not lead to significant changes in kinetic parameters compared to the acidic flow case devoid of these compounds and that only during uncaging were differences in N observed.

Assessment of Changes in the Extent of Fusion. To ensure that there was no artifact in the kinetic analysis resulting from a reduction in extent of fusion by the proton uncaging method, we compared the extents of fusion between the acidic buffer exchange experiments and the uncaging method. We found that the overall number of virions fusing in a given experiment at a given pH were similar (Table 2). This result shows that the

Table 2. Extent of Virus Fusion Obtained with Various Fusion Initiation Methods

fusion initiation method	extent of fusion (%)
14 mM <i>o</i> -NBA uncaging	27 ± 5
pH 4.5 acid flow exchange	17 ± 6
pH 4.7 acid flow exchange	25 ± 7

uncaging process has enough power to initiate the fusion of any virus present in the UV beam during the short pulse duration. We corroborated this result by irradiating the same area with a second UV pulse and found that no more fusion was initiated within a given region. Even though the UV pulse is short-lived, we obtain the same extent of fusion and hemifusion rate constants with uncaging as we obtain with the buffer exchange method; only N differs. Previous studies of influenza X:31 fusion after neutralization immediately following acidification show that, once the fusion protein is "activated," the rest of the process does not necessarily require a low pH environment.^{13,14} Therefore, the similarity of the fusion extents and hemifusion rate constants we obtain by these different acidification methods also corroborates these reports in the literature that the intermediate fusion steps are not strongly pH dependent.

Impact of the Method and Rate of Proton Delivery to the Fusion Proteins on Kinetics. The final possibility that could explain the lower value of N is the immediate availability of protons to fusion proteins upon uncaging compared to the acidic flow experiments. As N is in the exponent of the gamma fitting equation, it will be quite sensitive to initiation time. In the case of uncaging, the acidification to the target pH is rapid: the drop is complete after the 200 ms UV pulse. In contrast, the

time to drop the pH by the acidic buffer flow exchange is significantly longer (order of seconds) due to the no slip boundary condition at the bilayer surface. The impact of faster proton delivery on kinetics could be manifested in several ways. First, immediate availability of protons at the fusion protein ensures the coordination of initiation of fusion events at a specific pH value; second, faster acidification means better precision in knowing the time when acidification actually occurred (time = 0) for more certainty in determining lag times used in kinetic analysis.

To speed up the delivery of protons by acidic buffer exchange to better coordinate events, we carried out experiments at higher flow rates (500 $\mu\text{L}/\text{min}$) to ascertain the difference in the data and fits, as shown in Figure 6. With faster flow rate, we

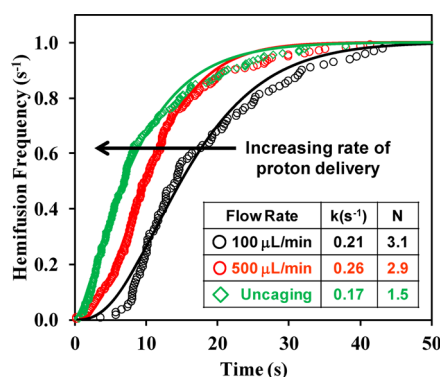


Figure 6. Fusion data at an initiation pH of 4.7. As the flow rate increases, the data trends shift closer to the uncaging data.

do observe a shift in the data toward the uncaging trend and a decrease in N ; however, the effect is small with only a 5-fold change in flow rate. We are precluded from increasing the flow rate much more in an attempt to match the uncaging value because the increased hydrodynamic shear on the bound virions starts to disrupt their attachment to the bilayer and significant shear may also lead to changes in kinetics as the HA may stretch and alter the binding pocket for the proton.

CONCLUSION

The dynamics of the HA protein conformational changes measured by variations in intrinsic tryptophan fluorescence are known to be on the millisecond time scale near pH 5.0.²⁶ While at the "optimal" pH (4.9), the protein conformational change is not thought to be the rate-limiting step in the fusion process; at "suboptimal" pHs (5.1 and above), a slower transition to the fusogenic conformational form of HA could explain slower fusion kinetics.²⁶ To eliminate proton transport effects on the measurement of the fusion kinetic parameters at "suboptimal" fusion pHs greater than 5.0, we used a proton uncaging strategy. The immediate availability of protons not only reduces or eliminates proton transport limitations but also synchronizes individual initiation times, increasing the resolution of the measurements obtained from analysis of the hemifusion data. Our data are consistent with the prevailing mechanism for influenza fusion mediated by HA, and the main finding here is that the number of trimers required for fusion is closer to two rather than three.

The commercially available *o*-NBA compound employed in this work is limited by its solubility in aqueous solutions to yielding a maximum change in pH from 7.0 to ~ 4.5 ; thus, we

did not examine fusion below pH 4.5. We note that, under physiological conditions, influenza fusion occurs within this pH range in the endosome. However, other more soluble proton caged compounds can be synthesized^{48,49} and used to study fusion at lower pH values using the uncaging method, which may be advantageous for studying other virus strains. Additionally, this approach is adaptable to studies of other membrane fusion processes (e.g., SNARE-mediated fusion) by changing the effector molecule to calcium,^{50,51} for example.

The impact of this work from a practical standpoint is that obtaining higher temporal resolution measurements of kinetic parameters between different virus strains aids in characterizing mutations that lead to enhanced fusion and viral infection. Furthermore, the fusion step, and in particular the HA protein, has become a target for antiviral drug development. Antifusogenic drugs, such as *tert*-butyl hydroquinone have been shown to strongly interact with the HA binding pocket to stabilize the neutral pH structure, which then presumably inhibits the conformational changes required for membrane fusion,³ and more recently, antibodies have been developed that target the stem region of the HA and are expected to disrupt fusion activity.^{52,53} With the method described here, the inhibition of viral fusion using these compounds could be tested directly and at a level of detail not available to date. This information will further refine antiviral drug design and characterization.

■ ASSOCIATED CONTENT

● Supporting Information

Materials and suppliers, buffer preparations, surface preparation, microfluidic device fabrication, supported bilayer preparation and characterization, virus labeling and purification, fluorescence dequenching, and image processing. This material is available free of charge via the Internet at <http://pubs.acs.org>.

■ AUTHOR INFORMATION

Corresponding Author

*Tel: 607-255-4675. Fax: 607-255-9166. E-mail: sd386@cornell.edu.

Notes

The authors declare no competing financial interest.

■ ACKNOWLEDGMENTS

We thank the NIAID Centers of Excellence for Influenza Research and Surveillance (CEIRS) and, in particular, the New York Influenza Center of Excellence (NYICE) pilot program at the University of Rochester (grant 414529-G to S.D. and L.P.), the Nanobiotechnology Center at Cornell University (to L.P., G.R.W., and S.D.), the National Institutes of Health (grant R01 AI48678 to G.R.W.), and start-up funds from Cornell University (to S.D.) for supporting this work.

■ REFERENCES

- (1) Wilschut, J.; Hoekstra, D., Eds. *Membrane Fusion*; Marcel Dekker, Inc.: New York, NY, 1991.
- (2) Skehel, J. J.; Wiley, D. C. *Annu. Rev. Biochem.* **2000**, *69*, 531–569.
- (3) Russell, R. J.; Kerry, P. S.; Stevens, D. J.; Steinhauer, D. A.; Martin, S. R.; Gambin, S. J.; Skehel, J. J. *Proc. Natl. Acad. Sci.* **2008**, *105*, 17736–17741.
- (4) Hoekstra, D.; de Boer, T.; Klappe, K.; Wilschut, J. *Biochemistry* **1984**, *23*, 5675–5681.
- (5) Hoekstra, D.; Klappe, K. *Methods Enzymol.* **1993**, *220*.

- (6) Chernomordik, L. V.; Leikina, E.; Frolov, V.; Bronk, P.; Zimmerberg, J. *J. Cell Biol.* **1997**, *136*, 81–93.
- (7) Polozov, I. V.; Berrukov, L.; Gawrisch, K.; Zimmerberg, J. *Nat. Chem. Biol.* **2008**, *4*, 248–255.
- (8) Ramalho-Santos, J.; Nir, S.; Duzgunes, N.; Pato de Carvalho, A.; da Conceicao Pedrosa de Lima, M. *Biochemistry* **1993**, *32*, 2771–2779.
- (9) Clague, M. J.; Schoch, C.; Blumenthal, R. *J. Virol.* **1991**, *65*, 2402–2407.
- (10) Stegmann, T.; Hoekstra, D.; Scherphof, G.; Wilschut, J. *Biochemistry* **1985**, *24*, 3107–3113.
- (11) Korte, T.; Ludwig, K.; Huang, Q.; Rachakonda, P. S.; Herrmann, A. *Eur. Biophys. J.* **2007**, *36*, 327–335.
- (12) Bentz, J. *Biophys. J.* **1992**, *63*, 448–459.
- (13) Stegmann, T.; White, J. M.; Helenius, A. *EMBO J.* **1990**, *9*, 4231–4241.
- (14) Blumenthal, R.; Schoch, C.; Puri, A.; Clague, M. *J. Ann. N.Y. Acad. Sci.* **1991**, *635*, 285–296.
- (15) Niles, W. D.; Cohen, F. S. *Biophys. J.* **1993**, *65*, 171–176.
- (16) Georgiou, G. N.; Morrison, I. E. G.; Cherry, R. J. *FEBS Lett.* **1989**, *250*, 487–492.
- (17) Niles, W. D.; Cohen, F. S. *J. Gen. Physiol.* **1991**, *97*, 1101–1119.
- (18) Sarkar, D. P.; Morris, S. J.; Eidelman, O.; Zimmerberg, J.; Blumenthal, R. *J. Cell Biol.* **1989**, *109*, 113–122.
- (19) Axelrod, D.; Burghardt, T. P.; Thompson, N. L. *Annu. Rev. Biophys. Bioeng.* **1984**, *13*, 247–268.
- (20) Floyd, D. L.; Ragain, J. R.; Skehel, J. J.; Harrison, S. C.; van Oijen, A. M. *Proc. Natl. Acad. Sci.* **2008**, *105*, 15382–15387.
- (21) Wessels, L.; Elting, M. W.; Scimeca, D.; Weninger, K. *Biophys. J.* **2007**, *93*, 526–538.
- (22) McCray, J. A.; Trentham, D. R. *Annu. Rev. Biophys. Biochem.* **1989**, *18*, 239–270.
- (23) Dantzig, J. A.; Higuchi, H.; Goldman, Y. E. *Methods Enzymol.* **1998**, *291*, 307–348.
- (24) Abbruzzetti, S.; Viappiani, C.; Small, J. R.; Libertini, L. J.; Small, E. W. *J. Am. Chem. Soc.* **2001**, *123*, 6649–6653.
- (25) Saxena, A. M.; Udgaonkar, J. B.; Krishnamoorthy, G. *Protein Sci.* **2005**, *14*, 1781–1799.
- (26) Krumbiegel, M.; Herrman, A.; Blumenthal, R. *Biophys. J.* **1994**, *67*, 2355–2360.
- (27) Loyter, A.; Citovsky, V.; Blumenthal, R. *Methods Biochem. Anal.* **1988**, *33*, 129–186.
- (28) Stober, F.; Fink, A.; Bohn, E. J. *J. Colloid Interface Sci.* **1968**, *26*, 62–69.
- (29) Ow, H.; Larson, D. R.; Srivastava, M.; Barird, B. A.; Webb, W. W.; Wiesner, U. *Nano Lett.* **2005**, *5*, 113–117.
- (30) Burns, A.; Sengupta, P.; Zedayko, T.; Baird, B.; Wiesner, U. *Small* **2006**, *2*, 723–726.
- (31) Hidalgo, G.; Burns, A.; hay, A.; Houston, P. L.; Wiesner, U.; Lion, L. W. *Appl. Environ. Microbiol.* **2009**, *75*, 7426–7435.
- (32) Brian, A. A.; McConnell, H. M. *Proc. Natl. Acad. Sci.* **1984**, *81*, 6159–6163.
- (33) Mao, H.; Yang, T.; Cremer, P. S. *Anal. Chem.* **2002**, *74*, 379–385.
- (34) Yang, T.; Jung, S.-Y.; Mao, H.; Cremer, P. S. *Anal. Chem.* **2001**, *73*, 165–169.
- (35) George, M. V.; Scaiano, J. C. *J. Phys. Chem.* **1980**, *84*, 492–495.
- (36) Harrison, S. C. *Nat. Struct. Mol. Biol.* **2008**, *15*, 690–698.
- (37) Tamm, L. K.; Crane, J.; Kiessling, V. *Curr. Opin. Struct. Biol.* **2003**, *13*, 453–466.
- (38) Larson, D. R.; Ow, H.; Vishwasrao, H. D.; Heikal, A. A.; Wiesner, U.; Webb, W. W. *Chem. Mater.* **2008**, *20*, 2677–2684.
- (39) Haugland, R. P. *The Handbook: A Guide to Fluorescent Probes and Labeling Technologies*; 10th ed.; Invitrogen Corp.: Eugene, OR, 2005.
- (40) Choi, J.; Hirota, N.; Terazima, M. *J. Phys. Chem. A* **2001**, *105*, 12–18.
- (41) Markovic, I.; Leikina, E.; Zhukovsky, M.; Zimmerberg, J.; Chernomordik, L. V. *J. Cell Biol.* **2001**, *155*, 833–843.

- (42) Ramalho-Santos, J.; Pedroso de Lima, M. C. *BBA* **1998**, *1376*, 147–154.
- (43) Danieli, T.; Pelletier, S. L.; Henis, Y. I.; White, J. M. *J. Cell Biol.* **1996**, *133*, 559–569.
- (44) Imai, M.; Mizuno, T.; Kawasaki, K. *J. Biol. Chem.* **2006**, *281*, 12729–12735.
- (45) Blumenthal, R.; Sarkar, D. P.; Durell, S.; Howard, D. E.; Morris, S. J. *J. Cell Biol.* **1996**, *135*, 63–71.
- (46) Dobay, M. P.; Dobay, A.; Bantang, J.; Mendoza, E. *Mol. BioSyst.* **2011**, *7*, 2741–2749.
- (47) Redfield, D. C.; Richman, D. D.; Oxman, M. N.; Kronenberg, L. H. *Infect. Immun.* **1981**, *32*, 1216–1226.
- (48) Janko, K.; Reichert, J. *Biochim. Biophys. Acta* **1987**, *905*, 409–416.
- (49) Barth, A.; Corrie, E. T. *Biophys. J.* **2002**, *83*, 2864–2871.
- (50) Brown, E. B.; Shear, J. B.; Adams, S. R.; Tsien, R. Y.; Webb, W. W. *Biophys. J.* **1999**, *76*, 489–499.
- (51) Burgalossi, A.; Jung, S.-Y.; Meyer, G.; Jockusch, W. J.; Jahn, O.; Taschenberger, H.; O'Connor, V. M.; Nishiki, T.-i.; Takahashi, M.; Brose, N.; Rhee, J.-S. *Neuron* **2010**, *68*, 473–487.
- (52) Corti, D.; Voss, J.; Gamblin, S. J.; Codoni, G.; Macagno, A.; Jarrossay, D.; Vachieri, S. G.; Pinna, D.; Minola, A.; Vanzetta, F.; Silacci, C.; Fernandez-Rodriguez, B. M.; Agatic, G.; Bianchi, S.; Giacchetto-Sasselli, I.; Calder, L.; Sallusto, F.; Collins, P.; Haire, L. F.; Temperton, N.; Langedijk, J. P. M.; Skehel, J. J.; Lanzavecchia, A. *Science* **2011**, *333*, 850–856.
- (53) Ekiert, D. C.; Friesen, R. H. E.; Bhabha, G.; Kwaks, T.; Jongeneelen, M.; Yu, W.; Ophorst, C.; Cox, F.; Korse, H. J. M. M.; Brandenburg, B.; Vogels, R.; Brakenhoff, J. P. J.; Kompier, R.; Koldijk, M. H.; Cornelissen, L. A. H. M.; Poon, L. L. M.; Peiris, M.; Koustaal, W.; Wilson, I. A.; Goudsmit, J. *Science* **2011**, *333*, 843–850.